catalysts

MDPI

Article

Comparison of Efficiencies and Mechanisms of Catalytic Ozonation of Recalcitrant Petroleum Refinery Wastewater by Ce, Mg, and Ce-Mg Oxides Loaded Al_2O_3

Chunmao Chen [1,†], Yu Chen [1,†], Brandon A. Yoza [2], Yuhao Du [1], Yuxian Wang [1], Qing X. Li [3], Lanping Yi [1], Shaohui Guo [1] and Qinghong Wang [1,*]

1 State Key Laboratory of Heavy Oil Processing, State Key Laboratory of Petroleum Pollution Control, China University of Petroleum, Beijing 102249, China; chunmaochan@163.com (C.C.); chenyu7@cnooc.com.cn (Y.C.); sam.duyuhao@gmail.com (Y.D.); yuxian.wang@cup.edu.cn (Y.W.); lanpingyi1995@gmail.com (L.Y.); cupgsh@163.com (S.G.)

2 Hawaii Natural Energy Institute, University of Hawaii at Manoa, Honolulu, HI 96822, USA; byoza@hawaii.edu

3 Department of Molecular Biosciences and Bioengineering, University of Hawaii at Manoa, Honolulu, HI 96822, USA; qingl@hawaii.edu

* Correspondence: wangqhqh@cup.edu.cn; Tel.: +86-10-8973-3771

† These authors contributed equally to this work.

Academic Editors: Shaobin Wang and Xiaoguang Duan

Received: 21 December 2016; Accepted: 21 February 2017; Published: 24 February 2017

Abstract: The use of catalytic ozonation processes (COPs) for the advanced treatment of recalcitrant petroleum refinery wastewater (RPRW) is rapidly expanding. In this study, magnesium (Mg), cerium (Ce), and Mg-Ce oxide-loaded alumina (Al_2O_3) were developed as cost efficient catalysts for ozonation treatment of RPRW, having performance metrics that meet new discharge standards. Interactions between the metal oxides and the Al_2O_3 support influence the catalytic properties, as well as the efficiency and mechanism. Mg-Ce/Al_2O_3 (Mg-Ce/Al_2O_3-COP) reduced the chemical oxygen demand by 4.7%, 4.1%, 6.0%, and 17.5% relative to Mg/Al_2O_3-COP, Ce/Al_2O_3-COP, Al_2O_3-COP, and single ozonation, respectively. The loaded composite metal oxides significantly increased the hydroxyl radical-mediated oxidation. Surface hydroxyl groups (–OHs) are the dominant catalytic active sites on Al_2O_3. These active surface –OHs along with the deposited metal oxides (Mg^{2+} and/or Ce^{4+}) increased the catalytic activity. The Mg-Ce/Al_2O_3 catalyst can be economically produced, has high efficiency, and is stable under acidic and alkaline conditions.

Keywords: petroleum refinery wastewater; catalytic ozonation; metal oxide; hydroxyl group

1. Introduction

Petroleum refinery wastewater (PRW) contains high levels of oil and petroleum-derived chemicals [1]. Treatment of PRW prior to discharge is needed to minimize adverse impacts on human and environmental health. After physico-chemical and biological treatments, PRW effluents from treatment plants previously met the Wastewater Discharge Standard of China (GB 8978-1996). However, due to increased regulations, they currently do not meet the recently revised Emission Standard of Pollutants for the Petroleum Refining Industry of China (GB 31570-2015), and they now require additional treatments. Biological treatment strategies are not applicable toward PRW reclamation, as the chemicals of concern are often present in low concentration and are recalcitrant [2,3].

Catalytic ozonation processes (COPs) have been identified as efficient methods for the removal of recalcitrant chemicals [4,5]. A wide variety of catalysts are used during COPs for this

purpose. However, synthesis and preparation are cost-intensive, limiting industrial applications. As economical supports, activated carbon (AC) and alumina (Al_2O_3) have good adsorption and catalytic performances [6–9]. Active components loaded onto AC and Al_2O_3 can further enhance the catalytic efficiency and result in better affordability. Metal oxides including manganese (Mn) [10], iron (Fe) [11], magnesium (Mg) [12], and cerium (Ce) [7,13] were found to significantly enhance chemical removal in wastewaters when deposited onto AC. The use of low-cost reclaimed carbon-containing wastes such as sewage sludge [14] and plastics [15] can make AC catalyst use cost-efficient. However, AC catalysts lack durability, strength, and stability, which reduce their application potential.

Al_2O_3 catalysts have shown excellent mechanical properties and catalytic efficiency [16,17]. The loading of metal oxides including Mn [18], Fe [19,20], nickel [21], and ruthenium [22] on Al_2O_3 has significantly increased the efficiency of ozonation for the treatment of recalcitrant compounds including pharmaceuticals, dimethyl phthalate, 4-dichlorophenoxy, propionic acid, nitrobenzene, and oxalic acid. Composite metal oxides loaded onto Al_2O_3 can also enhance catalytic activity relative to single metal oxides [23,24]. The use of Al-containing wastes such as red mud [25] and spent catalysts [26] as raw materials, and the development of efficient metallic catalysts can further increase cost efficiency. Ce oxides are widely used in COPs owing to their biological and chemical inertness, strong oxidation power, and cyclic usability [13,27]. Ce oxides doped or loaded on AC [13], red mud [25], SBA-15 [28], and MCM-41 [29] zeolites were effective at reducing pharmaceutical compounds, bezafibrate, dimethyl phthalate, and *p*-chlorobenzoic. MgO nanocrystals [30] and MgO-loaded granular AC [12] have also shown potential use for ozonation treatment and are effective for the treatment of azo dyes and catechol. However, Mg and/or Ce oxide-loaded Al_2O_3 as catalysts have not been previously reported for COP treatment of recalcitrant compounds. Furthermore, few studies have actually applied COPs toward the treatment of real recalcitrant PRW (RPRW) samples. Natural manganese sand ore was economical, but had low efficiency (35.7% removal of chemical oxygen demand (COD) for 90 min) [31]. The spent fluid catalytic cracking catalyst was cost-efficient, but it was difficult to maintain the catalytically active components [26].

Catalytic ozonation often involves a variety of oxidation mechanisms. Decomposition of ozone to more active hydroxyl radical (•OH) species and/or adsorbing chemicals to proximally react with dissolved ozone is the predominant catalytic mechanism that has the greatest impact [16,32]. Protonated surface hydroxyl groups (–OHs) on MnO_x/SBA-15 promote •OHs generation, and thus enhance the ozonation of norfloxacin [33]. The formation of surface complexes such as cobalt(II)-carboxylic acid accelerates the removal of *p*-chlorobenzoic in cobalt(II) oxide-aided ozonation [34]. Lewis acid sites on β-FeOOH/Al_2O_3 are reactive centers for the ozonation of pharmaceuticals [35]. The surface basic groups on MgO enhance the transformation rate of ozone to •OHs during the ozonation of 4-chlorophenol [36]. TiO_2/Al_2O_3 promotes the ozonation of oxalic acid by adsorbing oxalic acid and allowing it to directly react with ozone in solution in contrast to •OH-mediated oxidation [37]. Studies of COPs have currently been focused on model compounds. Few studies have used actual RPRW.

In this study, Mg, Ce, and Mg-Ce oxides loaded onto Al_2O_3 (Mg/Al_2O_3, Ce/Al_2O_3, and Mg-Ce/Al_2O_3, respectively) catalysts were prepared and characterized. The catalytic efficiency, mechanism, and potential of the prepared catalysts for COP treatment of RPRW were investigated.

2. Results and Discussion

2.1. Characteristics of Catalysts

X-ray diffraction (XRD) patterns for Al_2O_3, Mg/Al_2O_3, Ce/Al_2O_3, Mg-Ce/Al_2O_3 (I), and Mg-Ce/Al_2O_3 (II) all showed similar peak characteristics that are associated with Al_2O_3 at about 38°, 46° and 67° (Figure 1). Obvious XRD diffraction peaks of metal oxides were not observed due to the high dispersion and low concentration of the metal oxides.

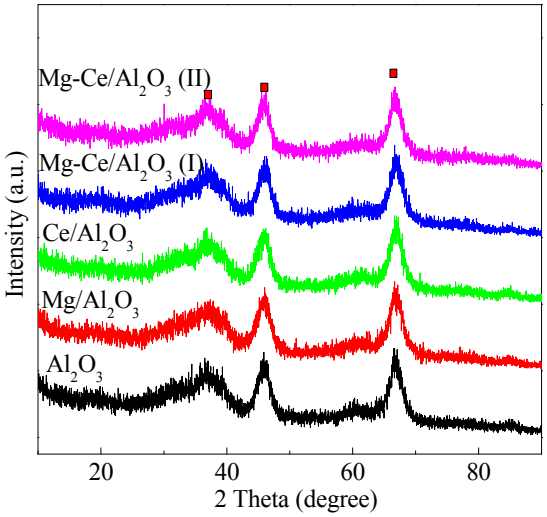

Figure 1. XRD patterns of Al_2O_3 and metal oxide-loaded Al_2O_3 catalysts.

Deposited Mg and/or Ce oxides formed micro-agglomerates in irregular shapes and sizes (Figure 2). The adsorption-desorption isotherms (Figure 3a) and pore distributions (Figure 3b) varied slightly among the different examined catalysts. According to the International Union of Pure and Applied Chemistry (IUPAC) classification, the isotherms suggest the presence of a typical type IV mesopore structure [38]. The surface areas (S_{BET}), pore volumes (V_P), and average pore sizes (D_a) were in the range of 245–250 m^2/g, 0.36–0.38 m^3/g, and 5.9–6.1 nm, respectively (Table 1). The contents of MgO and CeO_2 in Mg/Al_2O_3 or Ce/Al_2O_3 were 0.3 wt %. The contents of MgO and CeO_2 in $Mg\text{-}Ce/Al_2O_3$ (I) were both 0.3 wt % and those in $Mg\text{-}Ce/Al_2O_3$ (II) were both 0.9 wt % (Table 1). The low loadings of Mg and/or Ce oxides decreased the intensity of the functional surface groups (Figure 4a). The point zero charges (pH_{pzc}) of unloaded and loaded Al_2O_3 had only small differences, ranging from 8.1 to 8.3 (Figure 4b).

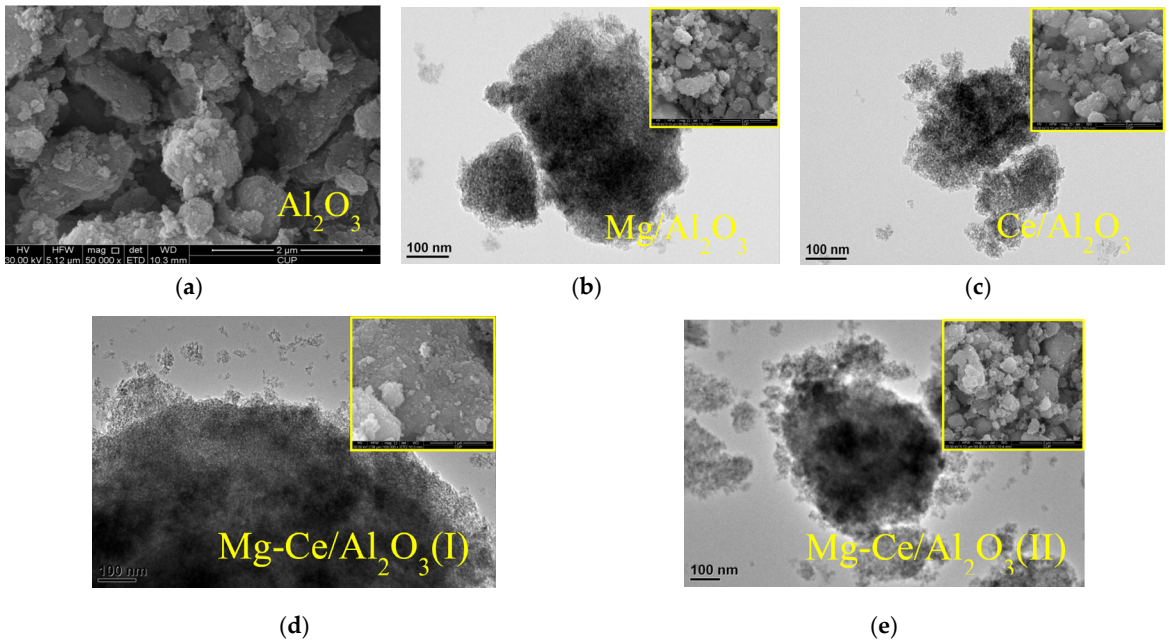

Figure 2. Scanning electron microscope (SEM) image of Al_2O_3 substrate (**a**) and transmission electron microscope micrographs of loaded Al_2O_3 with inset SEM images: (**b**) Mg/Al_2O_3; (**c**) Ce/Al_2O_3; (**d**) $Mg\text{-}Ce/Al_2O_3$ (I); (**e**) $Mg\text{-}Ce/Al_2O_3$ (II).

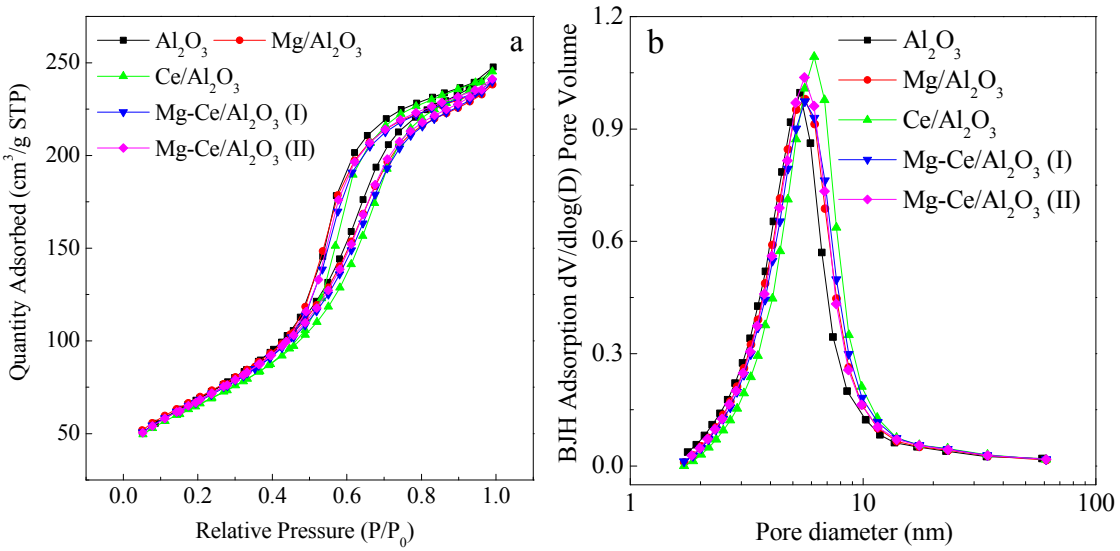

Figure 3. Isotherms (**a**) and pore distribution curves (**b**) using N_2 adsorption-desorption of Al_2O_3 and metal oxide-loaded Al_2O_3 catalysts.

Table 1. Surface areas, pore structures, and metal oxide contents of Al_2O_3 and metal oxide-loaded Al_2O_3 catalysts.

Catalysts	Surface Areas and Pore Structures			Metal Oxide Contents (wt %)	
	S_{BET} (m^2/g)	V_P (cm^3/g)	D_a (nm)	MgO	CeO_2
Al_2O_3	250	0.36	6.1	-	-
Mg/Al_2O_3	250	0.38	5.9	0.30	-
Ce/Al_2O_3	246	0.38	6.1	-	0.31
$Mg\text{-}Ce/Al_2O_3$ (I)	245	0.38	6.0	0.31	0.33
$Mg\text{-}Ce/Al_2O_3$ (II)	246	0.37	6.1	0.92	0.90

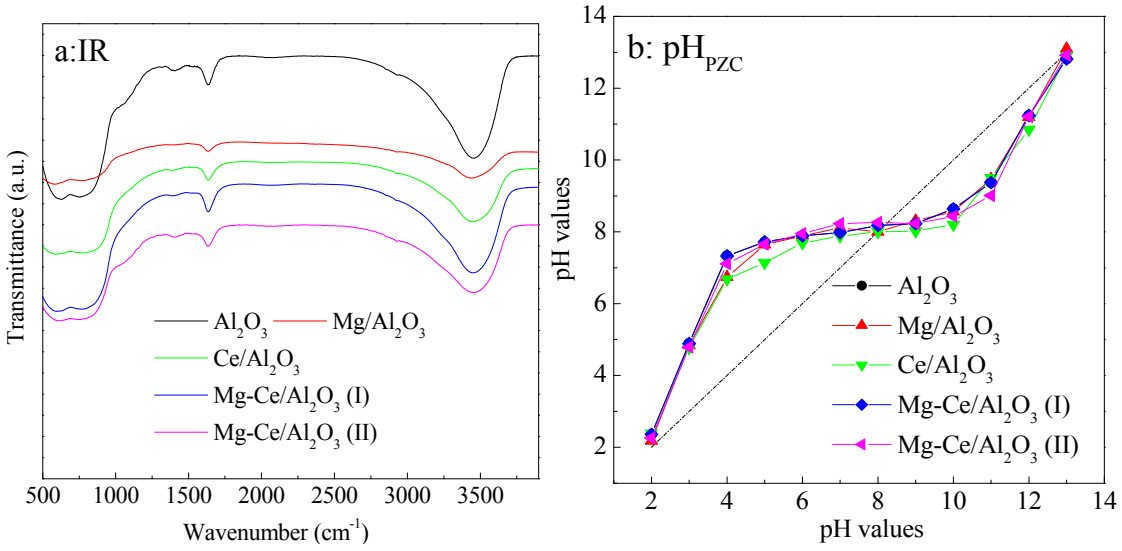

Figure 4. Infrared (IR) spectra (**a**) and pH_{pzc} values (**b**) of Al_2O_3 and metal oxide-loaded Al_2O_3 catalysts.

Figure 5 illustrates the UV-vis spectra for the prepared catalysts. Al_2O_3 showed an absorption peak at around 260 nm. Mg/Al_2O_3 exhibited a strong absorption centered at 200 nm and a wider low-intensity absorption profile at 220–380 nm. The large initial absorption peak is associated with

micro-aggregates from highly dispersed Mg^{2+} on the Al_2O_3 surface and the lower broad profile due to the Al_2O_3 substrate [12]. Ce/Al_2O_3 had a broad 200–380 nm absorption profile with a peak at 260 nm, which can be associated with overlapping transitional charge transfers that occur between $O^{2-} \rightarrow Ce^{4+}$ [39]. Mg-Ce/Al_2O_3 (I) and Mg-Ce/Al_2O_3 (II) both exhibited stronger absorption profiles between 200 and 380 nm and had a similar peak at 260 nm, which can be attributed to increased concentrations of deposited metal oxides and also to the interactions between them.

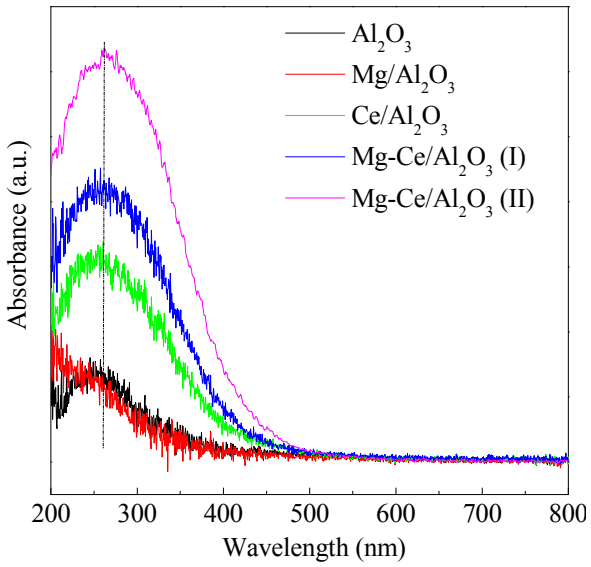

Figure 5. UV-vis patterns of Al_2O_3 and metal oxide-loaded Al_2O_3 catalysts.

Figure 6a presents the Mg1s spectra of catalysts based on X-ray photoelectron spectroscopy (XPS). The binding energy of Mg1s from Mg^{2+} oxides was centered at 1303 eV [40]. The asymmetrical distribution of the Mg1s peak for Mg/Al_2O_3 was likely due to strong interactions between Mg and the Al_2O_3 support. For Mg/Al_2O_3, the surface content of MgO (0.71 wt %) was greater than the bulk content (0.30 wt %), suggesting surface enrichment. Mg-Ce/Al_2O_3 (I) displayed a similar Mg1s peak compared to Mg/Al_2O_3, having only a slight influence of Mg and Al_2O_3 interactions. The increased intensity of the Mg1s peak for Mg-Ce/Al_2O_3 (I) suggests that the surface distribution of Mg was enhanced through the introduction of Ce. The surface content of MgO (0.78 wt %) for Mg-Ce/Al_2O_3 (I) was higher than that (0.71 wt %) for Mg/Al_2O_3. Mg-Ce/Al_2O_3 (II) showed a symmetrical distribution of the Mg1s peak relative to Mg/Al_2O_3 and Mg-Ce/Al_2O_3 (I), suggesting a reduction of the Mg and Al_2O_3 interaction. The surface content of MgO for Mg-Ce/Al_2O_3 (II) was 0.75 wt %, similar to those of Mg/Al_2O_3 (0.71 wt %) and Mg-Ce/Al_2O_3 (I) (0.78 wt %), although the loading of MgO of the former was three-fold of the latter. This demonstrates that greater concentrations of MgO exist in bulk rather than being highly dispersed on the surface of Mg-Ce/Al_2O_3 (II).

The 3d XPS spectra for Ce are complex and usually exhibit 10 peaks having a range of binding energy between 880–920 eV: five spin-orbit split doublets corresponding to the 3d3/2 (high binding energy component) and 3d5/2 (low binding energy component) states. Figure 6b presents the 3d XPS spectra from Ce catalysts. The Ce/Al_2O_3 catalyst did not exhibit noticeable 3d peaks that are associated with CeO_2, likely due to the low surface distribution. Mg-Ce/Al_2O_3 (I) and Mg-Ce/Al_2O_3 (II), however, exhibited well-developed 3d peaks from the Ce^{4+} oxides [41]. The surface content of CeO_2 (0.67 wt %) on Mg-Ce/Al_2O_3 (I) was greater (0.40 wt %) relative to Ce/Al_2O_3 only (Table 2). The introduction of Mg further promoted the surface enrichment of Ce. This was also observed with Mg-Ce/Al_2O_3 (II). The surface content of CeO_2 on Mg-Ce/Al_2O_3 (II) increased to 2.57 wt % after triple CeO_2 loadings. The surface molar ratios (Mg1s + Ce3d/Al2p) of Mg-Ce/Al_2O_3 (I) and (II) were 0.012 and 0.0198, respectively, suggesting a highly disperse surface distribution of metal oxides, which is

supported by the XRD results. The surface molar ratio of Ce3d to Mg1s of Mg-Ce/Al_2O_3 (II) (0.8) increased in comparison to Mg-Ce/Al_2O_3 (I) (0.2). The increases likely enhanced the interactions between the Ce and Mg oxides on the surface of Mg-Ce/Al_2O_3 (II), relative to Mg-Ce/Al_2O_3 (I).

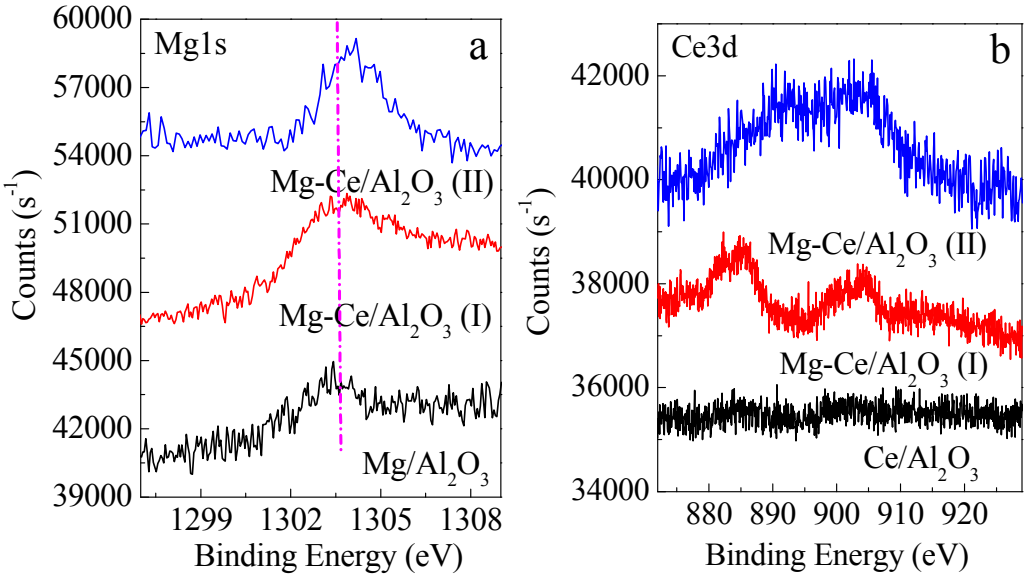

Figure 6. X-ray photoelectron spectroscopy (XPS) spectra of Mg1s (**a**) and Ce3d (**b**) of metal oxide-loaded Al_2O_3 catalysts.

Table 2. Molar ratios of Mg and Ce to Al, and surface contents of MgO and CeO_2 for catalysts by XPS analysis.

Items		Mg/Al_2O_3	Ce/Al_2O_3	Mg-Ce/Al_2O_3 (I)	Mg-Ce/Al_2O_3 (II)
Surface molar ratios	Mg1s/Al2p	0.009	-	0.010	0.0099
	Ce3d/Al2p	-	0.0012	0.002	0.0079
	Ce3d/Mg1s	-	-	0.2	0.8
	Mg1s + Ce3d/Al2p	0.009	0.0012	0.012	0.0198
Surface contents (wt %)	MgO	0.71	-	0.78	0.75
	CeO_2	-	0.40	0.67	2.57

2.2. *Efficiencies of Catalysts*

The catalytic COD reduction efficiency of RPRW was investigated by measuring the effect of adsorption, single ozonation and COPs. Adsorption on these catalysts was found to reach saturation within 40 min. The catalysts only weakly adsorbed target chemicals in RPRW and increased COD removal by only 6.3%–8.5% after 40 min (Figure 7a). Due to similar surface areas and pore structures, no significant differences in adsorption capacity among catalysts were observed (Table 1). After 40 min, COD removal by single ozonation, Al_2O_3-catalyzed ozonation (Al_2O_3-COP), Mg/Al_2O_3-COP, Ce/Al_2O_3-COP, Mg-Ce/Al_2O_3 (I)-COP, and Mg-Ce/Al_2O_3 (II)-COP was 34.3%, 45.9%, 47.2%, 47.8%, 51.9%, and 52.7%, respectively (Figure 7b). These results further support the fact that the catalytic process is driven primarily by ozonation rather than simple adsorption. Different COP treatments increased COD removal by 18.4%–11.6% compared with single ozonation. These differences are the results of catalytic metal oxide-driven ozonation processes. Mg-Ce/Al_2O_3 (I) exhibited a better performance compared with Mg/Al_2O_3 and Ce/Al_2O_3, while greater loadings of Mg and Ce were only slightly more effective. The surface areas and pore structures were comparable for these catalysts and they had only negligible differences on the results. The enhanced catalytic activity of Mg-Ce/Al_2O_3 (I) was due to interactions between the metal oxides, and between the metal oxides and the Al_2O_3 support, as well as their environments. The limited enhancement of catalytic activity for Mg-Ce/Al_2O_3 (II) was likely related to the presence of more MgO in bulk, as well as the partial occupation of

Al_2O_3 active surface sites by Mg and Ce oxides. No obvious leaching of Ce and Mg elements was detected in Mg-Ce/Al_2O_3 (I)-and (II)-COPs, suggesting good stability of the catalysts. COD removals of RPRW after 10 repeated uses of three COPs were monitored (Figure 7c). The Mg-Ce/Al_2O_3 (I)-COP (51.9%–50.7%) and Mg-Ce/Al_2O_3 (II)-COP (52.7%–49.6%) remained stable, suggesting high reusability and stability of the catalysts. The COD value from effluents after Mg-Ce/Al_2O_3 (I)-COP met the Emission Standard of Pollutants for the Petroleum Refining Industry of China (GB 31570-2015).

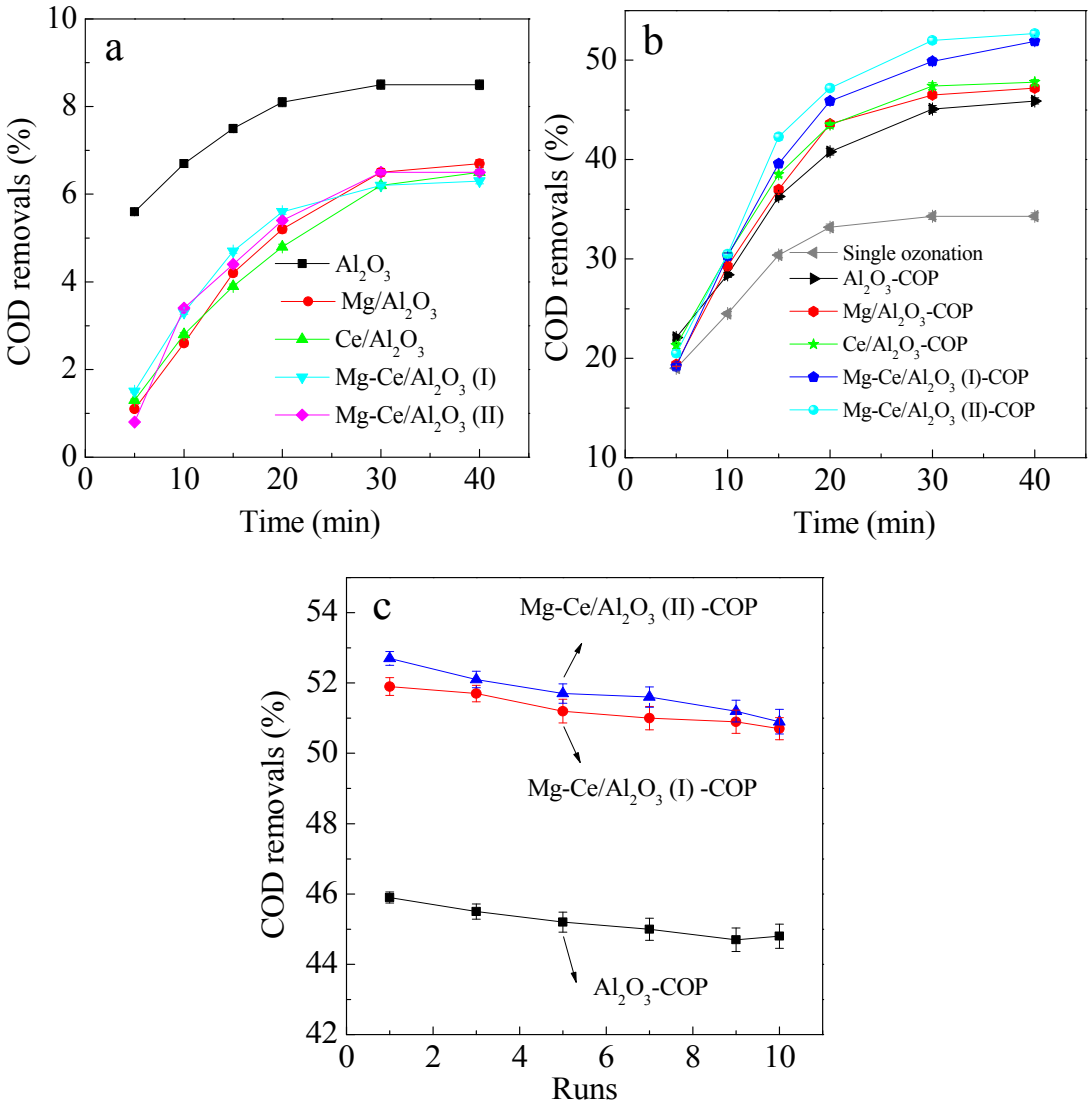

Figure 7. COD removals for RPRW by adsorption (**a**); by single ozonation and COPs (**b**); and by 10 repeated uses of COPs (**c**) (note: 0.5 g catalyst, 5 mg/min ozone, and 30 °C).

2.3. Mechanisms of Catalytic Ozonation

Numerous reports have suggested that •OH generation induced by various catalysts can promote the removal of chemicals during COPs. In order to determine whether •OH generation was occurring during COP treatment, *tert*-butanol (*t*BA) and sodium bicarbonate ($NaHCO_3$) were used as inhibitors during testing. The introduction of *t*BA and $NaHCO_3$ decreased the COD reduction efficiency (Figure 8). The results suggest that COD removal occurred primarily via •OH-mediated oxidation. The decreased extent of COD removal by both *t*BA and $NaHCO_3$ in Mg-Ce/Al_2O_3 (I)-COP and Mg-Ce/Al_2O_3 (II)-COP was greater than that of the other COPs. The results again suggest that the use of low concentrations of composite Mg and Ce deposited onto Al_2O_3 can further enhance •OH generation

compared to Mg/Al_2O_3 and Ce/Al_2O_3. COD reduction still occurred in spite of the addition of •OH scavengers, and was a result of direct ozonation.

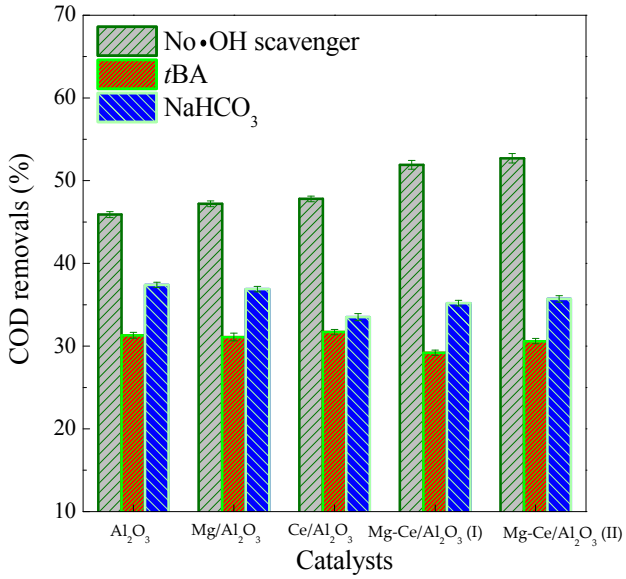

Figure 8. Influence of •OH scavengers (1 g/L) on COD removals of RPRW over COPs (note: 0.5 g catalyst, 5 mg/min ozone, 30 °C and 40 min; 1g/L •OH scavengers).

It is believed that active catalytic surfaces can induce ozone to form •OH, accelerating chemical degradation. Surface –OHs on the catalytic surface are known to have an impact during this process [42–44]. Solution pH values near the pH_{pzc} of a catalyst can result in accelerated •OH generation [45]. Initial pH values (about 4.06, 8.15, and 10.21) were examined and found to have a significant impact on COD removal efficiency during COP treatment (Figure 9).

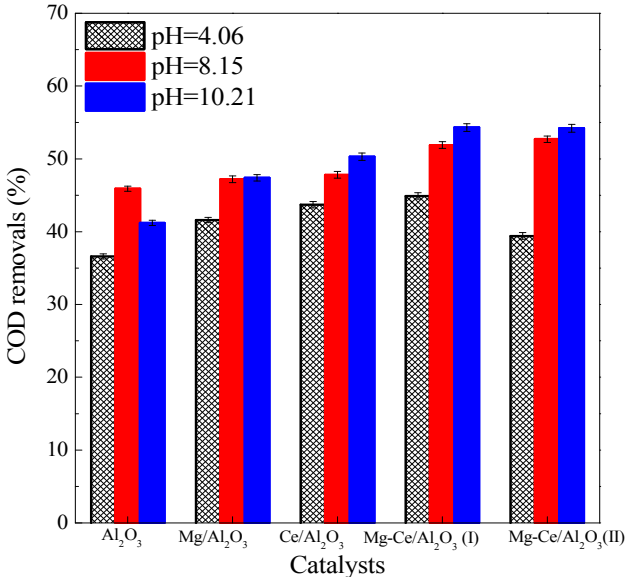

Figure 9. Influence of initial pH values on COD removals of RPRW over COPs (note: 0.5 g catalyst, 5 mg/min ozone, 30 °C and 40 min).

Low initial pH values around 4.06 resulted in low treatment efficiency, likely due to the direct oxidation of molecular ozone. Indirect oxidation was found to also occur at alkaline pH and was

a result of the •OH produced during ozone decomposition. Efficient COD removal was, however, high for five of the COP treatments, having an initial pH value around 8.15. Increasing such a pH value from 8.15 to 10.21 resulted in a decreased COD reduction efficiency for Al_2O_3-COP, but it was increased for Mg/Al_2O_3-COP, Ce/Al_2O_3-COP, Mg-Ce/Al_2O_3 (I)-COP, and Mg-Ce/Al_2O_3 (II)-COP. The magnitudes of surface –OHs from the greatest to smallest for the catalysts were Al_2O_3 > Mg/Al_2O_3 ≈ Mg-Ce/Al_2O_3 (I) > Ce/Al_2O_3 > Mg-Ce/Al_2O_3 (II), according to the O1s XPS spectra (Figure 10) [46].

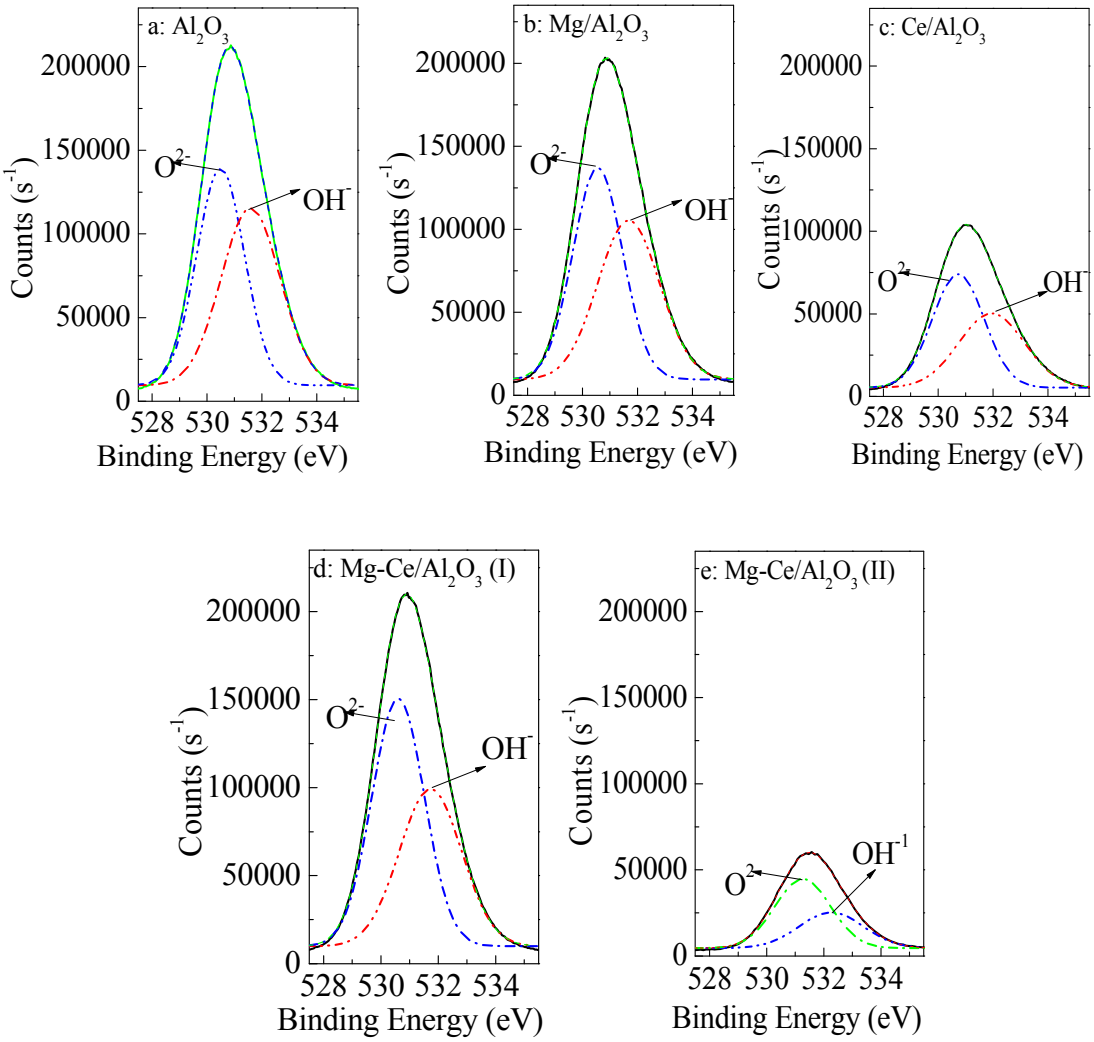

Figure 10. XPS spectra of O1s of Al_2O_3 and metal oxide-loaded Al_2O_3 catalysts. (**a**) Al_2O_3; (**b**) Mg/Al_2O_3; (**c**) Ce/Al_2O_3; (**d**) Mg-Ce/Al_2O_3 (I); (**e**) Mg-Ce/Al_2O_3 (II).

Al_2O_3-COP was the most efficient at an initial pH value of 8.15, close to its pH_{pzc} value (8.19), due to highly active surface –OHs. The other COPs were the most efficient at an initial pH value of 10.21, away from their pH_{pzc} values (8.1~8.3). This suggests that the active sites on the catalysts were modified due to the introduction of Mg and/or oxides on Al_2O_3. Mg/Al_2O_3 and Ce/Al_2O_3 exhibited higher COD removal efficiency in comparison to Al_2O_3, despite the lower surface –OHs. This illustrates the increased effect due to an increase in the dispersion of Mg or Ce oxides on the surface. Ce/Al_2O_3 had lower surface –OHs compared to Mg/Al_2O_3. Furthermore, the surface molar ratio of Ce3d/Al2p (0.0012) on Ce/Al_2O_3 was lower than that of Mg1s/Al2p (0.009) on Mg/Al_2O_3. However, a small increase in efficiency for COD removal using Ce/Al_2O_3 was observed when compared with Mg/Al_2O_3, suggesting higher Ce oxide catalytic activity over Mg^{2+} oxide. The increased COD removal for Mg-Ce/Al_2O_3 (I) and (II) was due to an enhanced surface distribution of the metal oxides when

compared to Mg/Al_2O_3 and Ce/Al_2O_3, despite the lower surface –OHs. For Mg/Al_2O_3, Ce/Al_2O_3, $Mg\text{-}Ce/Al_2O_3$ (I) and (II), dispersion of the Ce and/or Mg oxides increased available active sites and accelerated COD removal during the COP treatment. However, the activity contribution from surface –OHs is still important for the COP treatment, especially when the low surface loading of Ce and/or Mg oxides is considered. Therefore, the Ce and/or Mg oxides and surface –OHs likely have a co-functional activity on metal oxide-loaded Al_2O_3. At an initial pH value of 4.06, $Mg\text{-}Ce/Al_2O_3$ (II) exhibited low COD removal efficiency, suggesting poor acidic tolerance. For $Mg\text{-}Ce/Al_2O_3$ (II), interactions between MgO and the Al_2O_3 support are weak, causing the dissolution of MgO and nearby Ce^{4+} oxides under these acidic conditions. For Mg/Al_2O_3, Ce/Al_2O_3, and $Mg\text{-}Ce/Al_2O_3$ (I), interactions between the metal oxides and the Al_2O_3 support are strong, maintaining higher stability. The acid-resistant metal oxide-loaded Al_2O_3 catalysts exhibited higher COD removal efficiency compared to Al_2O_3 from an increase in direct oxidation. The metal oxide-loaded Al_2O_3 catalysts provided a platform for the adsorption of chemicals and/or ozone molecules, resulting in higher reactivities. These are strongly influenced by the surface metal oxide composition, the coordinated environmental distribution, and the interactions between the metal oxides and the Al_2O_3 support (Figure 11).

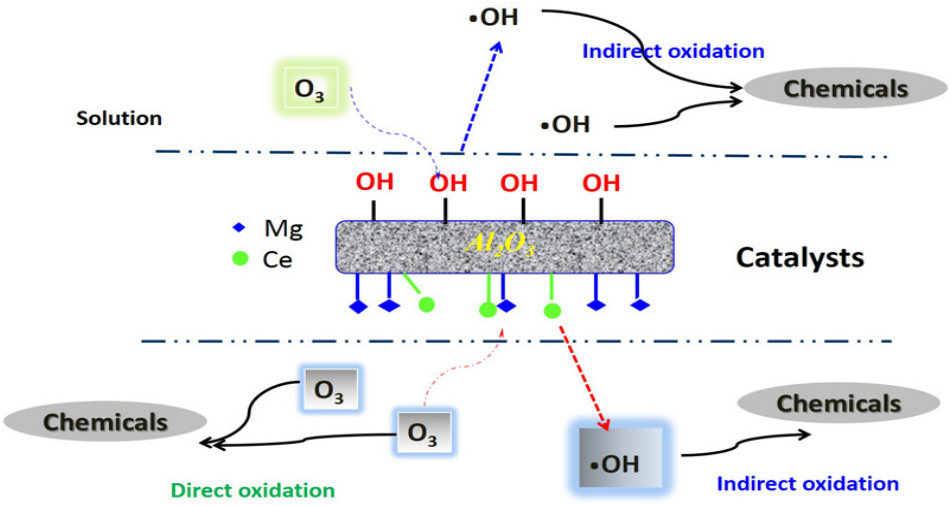

Figure 11. Proposed ozonation mechanisms of chemicals in RPRW upon metal oxide-loaded Al_2O_3 catalysts.

3. Materials and Methods

3.1. Preparation of Catalysts

Commercial pseudo bohemite (65.6 wt % of Al_2O_3) was purchased from Chalco Shandong Co., Ltd., Zibo, China. $Mg(NO_3)_2{\cdot}6H_2O$ (≥99.0 wt %) and $Ce(NO_3)_3{\cdot}6H_2O$ (≥99.0 wt %) were obtained from Beijing Chemical Reagents Co., Beijing, China. The catalysts were prepared according to the incipient wetness impregnation method. Impregnation of 60.00 g boehmite with the mixture solution of 0.76 g $Mg(NO_3)_2{\cdot}6H_2O$ and 0.33 g $Ce(NO_3)_3{\cdot}6H_2O$ yielded $Mg\text{-}Ce/Al_2O_3$(I) catalyst. Tripled $Mg(NO_3)_2{\cdot}6H_2O$ and $Ce(NO_3)_3{\cdot}6H_2O$ yielded $Mg\text{-}Ce/Al_2O_3$(II) catalyst. Impregnation of 60.00 g boehmite with 0.76 g $Mg(NO_3)_2{\cdot}6H_2O$ or 0.33 g $Ce(NO_3)_3{\cdot}6H_2O$ yielded Mg/Al_2O_3 or Ce/Al_2O_3 catalysts, respectively. The impregnated samples were calcinated at 550 °C for 4 h in air after drying at 90 °C for 12 h. Al_2O_3 was prepared from pseudo bohemite by calcination at 550 °C for 4 h in air.

3.2. Characterization of Catalysts

XRD was performed with a XRD-6000 powder diffraction instrument (Shimadzu, Kyoto, Japan) with a 40.0 kV working voltage and 40.0 mA electric current. The surface area and pore volume were determined with an ASAP2000 accelerated surface area and porosimetry system (Micromeritics,

Norcross, GA, USA). The composition was determined with a ZSX-100E X-ray fluorospectrometer (Rigaku, Tokyo, Japan). Surface element distribution was recorded with a PHI Quantera SXM X-ray photoelectron spectrometer (ULVACPHI, Chanhassen, MN, USA). The surface morphology was observed under a Quanta 200 F scanning electron microscope (FEI, Hillsboro, OR, USA) and a Tecnai G2 F20 transmission electron microscope (FEI). IR spectroscopy was determined on a MAGNA-IR560ESP FT-IR spectrometer (Nicolet, Madison, WI, USA). The diffuse reflectance spectra were recorded on a U-4100 UV-vis spectrophotometer (Hitachi, Tokyo, Japan). The pH_{pzc} of catalysts was determined according to the pH-drift procedure [47]. The leaching of Ce and Mg elements was measured with an AAnalyst atomic absorption spectrometer (PerkinElmer, Waltham, MA, USA) using a nitrous oxide/oxygen-acetylene flames.

3.3. Ozonation of RPRW

The RPRW was collected directly from the effluent of a bio-treatment unit of a wastewater treatment plant in CNOOC Huizhou Refining & Chemical Co., Ltd, Huizhou, China. The pH value, electric conductivity at 25 °C, BOD_5, and COD were 8.15, 3418 μs/cm, 20.24 mg/L, and 101.3 mg/L, respectively. The oils and biodegradable chemicals in RPRW have been removed after a long physicochemical and biological treatment. The chemical compositions in RPRW mainly were organic acids (27.42%), heterocyclic compounds (24.49%), alkanes (19.56%), esters (19.24%), and alcohols (4.79%) according to gas chromatography mass spectrometry analysis. Due to low biodegradability (BOD_5/COD ratio at 0.2), the COP was determined as an efficient advanced treatment method for the RPRW.

The experimental system was consisted of an oxygen tank, RQ-02 ozone generator (Ruiqing, China), 200 mL quartz column reactor, flow meter, and an exhaust gas collector. An aliquot of 100 mL of RPRW and 0.5 g catalyst were added in the reactor at 30 °C. The gaseous ozone was then introduced through a porous diffuser at the bottom of the reactor with a flow rate of 5 mg/min. The experiments were carried out using varying initial pH values (adjusted with 1 N NaOH or HCl) and reaction times. After treatment, dried oxygen was blown into the RPRW at a rate of 3.0 L/min to quench the reaction and eliminate the residual ozone. The resulting suspension was filtered (Whatman Qualitative No. 5) to separate catalyst particles prior to a further analysis. The •OH quenching experiments were performed to study the oxidation mechanism. The •OH scavengers, *t*BA and $NaHCO_3$ were added into RPRW (1.0 g/L) prior to experiments. All experiments were performed in triplicate.

The pH and electric conductivity were measured with a MP 220 pH meter (Mettler Toledo, Greifensee, Switzerland) and a CD400 electrical conductivity meter (Alalis, Shanghai, China), respectively. The BOD_5 was measured with a BODTrak II BOD meter (HACH, Loveland, CO, USA). The COD was measured with a CTL-12 COD meter (HATO, Chengde, China). The COD removal was calculated using the flowing equation:

$$\text{COD removal} = ([\text{COD}]_0 - [\text{COD}]_1)/[\text{COD}]_0 \quad (1)$$

4. Conclusions

Metal oxide-loaded Al_2O_3 catalysts were prepared, characterized and successfully evaluated for ozonation treatment of RPRW. Interactions between metal oxides and between the metal oxides and the Al_2O_3 support greatly influenced the surface structures and catalytic properties. The surface –OHs and metal oxides both function as active catalytic sites that promote •OH generation. Composite metal oxide-loaded Al_2O_3 exhibited higher efficiencies compared with single metal oxides. Mg-Ce/Al_2O_3-COP enhanced the COD removal by 4.7%, 4.1%, 6.0%, and 17.5%, respectively, in comparison with Mg/Al_2O_3-COP, Ce/Al_2O_3-COP, Al_2O_3-COP, and single ozonation. Our results suggest that an Mg-Ce/Al_2O_3 catalyst is commercially feasible, has high stability and can be cost-effective for ozonation treatment of RPRW.

Acknowledgments: This project was supported in part by the National Science and Technology Major Project of China (No. 2016ZX05040-003) and the National Natural Science Foundation of China (No. 21576287 and No. 21306229).

Author Contributions: Qinghong Wang and Chunmao Chen conceived and designed the experiments; Yu Chen and Yuhao Du performed the experiments; Yu Chen, Qing X. Li, Yuxian Wang, and Brandon A. Yoza interpreted and analyzed the data; Lanping Yi and Shaohui Guo contributed reagents/materials/analysis tools; Brandon A. Yoza, Qing X. Li, and Chunmao Chen wrote the manuscript.

Conflicts of Interest: The authors declare no conflict of interest.

References

1. Al Zarooni, M.; Elshorbagy, W. Characterization and assessment of Al Ruwais refinery wastewater. *J. Hazard. Mater.* **2006**, *136*, 398–405. [CrossRef] [PubMed]
2. Guo, X.; Zhan, Y.; Chen, C.M.; Zhao, L.; Guo, S. The influence of microbial synergistic and antagonistic effects on the performance of refinery wastewater microbial fuel cells. *J. Power Sources* **2014**, *251*, 229–236. [CrossRef]
3. EI-Naas, M.H.; Al-Zuhair, S.; Alhaija, M.A. Reduction of COD in refinery wastewater through adsorption on date-pit activate carbon. *J. Hazard. Mater.* **2009**, *173*, 750–757. [CrossRef] [PubMed]
4. Wu, J.; Ma, L.; Chen, Y.; Cheng, Y.; Liu, Y.; Zha, X. Catalytic ozonation of organic pollutants from bio-treated dyeing and finishing wastewater using recycled waste iron shavings as a catalyst: Removal and pathways. *Water Res.* **2016**, *92*, 140–148. [CrossRef] [PubMed]
5. Shahidi, D.; Roy, R.A. Advances in catalytic oxidation of organic pollutants—Prospects for thorough mineralization by natural clay catalysts. *Appl. Catal. B* **2015**, *174–175*, 277–292. [CrossRef]
6. Ma, J.; Sui, M.; Zhang, T.; Guan, C. Effect of pH on MnO_x/GAC catalyzed ozonation for degradation of nitrobenzene. *Water Res.* **2005**, *39*, 779–786. [CrossRef] [PubMed]
7. Li, L.; Ye, W.; Zhang, Q.; Sun, F.; Lu, P.; Li, X. Catalytic ozonation of dimethyl phthalate over cerium supported on activated carbon. *J. Hazard. Mater.* **2009**, *170*, 411–416. [CrossRef] [PubMed]
8. Qi, F.; Xu, B.; Chen, Z.; Ma, J.; Sun, D.; Zhang, L. Influence of aluminum oxides surface properties on catalyzed ozonation of 2,4,6-trichloroanisole. *Sep. Purif. Technol.* **2009**, *66*, 405–410. [CrossRef]
9. Vittenet, J.; Aboussaoud, W.; Mendret, J.; Pic, J.; Debellefontaine, H.; Lesagee, N.; Faucher, K.; Manero, M.H.; Thibault-Starzyk, F.; Leclerc, H.; et al. Catalytic ozonation with γ-Al_2O_3 to enhance the degradation of refractory organics in water. *Appl. Catal. A* **2015**, *504*, 519–532. [CrossRef]
10. Chen, C.; Wei, L.; Guo, X.; Guo, S.; Yan, G. Investigation of heavy oil refinery wastewater treatment by integrated ozone and activated carbon supported manganese oxides. *Fuel Process. Technol.* **2014**, *124*, 165–173. [CrossRef]
11. Chen, C.; Chen, H.; Guo, X.; Guo, S.; Yan, G. Advanced ozone treatment of heavy oil refining wastewater by activated carbon supported iron oxide. *J. Ind. Eng. Chem.* **2014**, *20*, 2782–2791. [CrossRef]
12. Moussavi, G.; Aghapour, A.A.; Yaghmaeian, K. The degradation and mineralization of catechol using ozonation catalyzed with MgO/GAC composite in a fluidized bed reactor. *Chem. Eng. J.* **2014**, *249*, 302–310. [CrossRef]
13. Dai, Q.; Wang, J.; Chen, J.; Chen, J. Ozonation catalyzed by cerium supported on activated carbon for the degradation of typical pharmaceutical wastewater. *Sep. Purif. Technol.* **2014**, *127*, 112–120. [CrossRef]
14. Zhuang, H.; Han, H.; Hou, B.; Jia, S.; Zhao, Q. Heterogeneous catalytic ozonation of biologically pretreated Lurgi coal gasification wastewater using sewage sludge based activated carbon supported manganese and ferric oxides as catalysts. *Bioresource Technol.* **2014**, *166*, 178–186. [CrossRef] [PubMed]
15. Dias, J.M.; Alvim-Ferraz, M.C.M.; Almeida, M.F.; Rivera-Utrilla, J.; Sa´nchez-Polo, M. Waste materials for activated carbon preparation and its use in aqueous-phase treatment: A review. *J. Environ. Manage.* **2007**, *85*, 833–846. [CrossRef] [PubMed]
16. Pocostales, P.; Álvarez, P.; Beltrán, F.J. Catalytic ozonation promoted by alumina-based catalysts for the removal of some pharmaceutical compounds from water. *Chem. Eng. J.* **2011**, *168*, 1289–1295. [CrossRef]
17. Roshani, B.; McMaster, I.; Rezaei, E.; Soltan, J. Catalytic ozonation of benzotriazole over alumina supported transition metal oxide catalysts in water. *Sep. Purif. Technol.* **2014**, *135*, 158–164. [CrossRef]
18. Yang, L.; Hu, C.; Nie, Y.; Qu, J. Catalytic ozonation of selected pharmaceuticals over mesoporous alumina-supported manganese oxide. *Environ. Sci. Technol.* **2009**, *43*, 2525–2529. [CrossRef] [PubMed]

19. Nie, Y.; Li, N.; Hu, C. Enhanced inhibition of bromate formation in catalytic ozonation of organic pollutants over Fe-Al LDH/Al_2O_3. *Sep. Purif. Technol.* **2015**, *151*, 256–261. [CrossRef]
20. Chen, K.C.; Wang, Y.H. The effects of Fe-Mn oxide and TiO_2/α-Al_2O_3 on the formation of disinfection by-products in catalytic ozonation. *Chem. Eng. J.* **2014**, *253*, 84–92. [CrossRef]
21. Avramescu, S.M.; Bradu, C.; Udrea, I.; Mihalache, N.; Ruta, F. Degradation of oxalic acid from aqueous solutions by ozonation in presence of Ni/Al_2O_3 catalysts. *Catal. Commun.* **2008**, *9*, 2386–2391. [CrossRef]
22. Wang, J.; Cheng, J.; Wang, C.; Yang, S.; Zhu, W. Catalytic ozonation of dimethyl phthalate with RuO_2/Al_2O_3 catalysts prepared by microwave irradiation. *Catal. Commun.* **2013**, *41*, 1–5. [CrossRef]
23. Chen, C.; Yoza, B.A.; Wang, Y.; Wang, P.; Li, Q.X.; Guo, S.; Yan, G. Catalytic ozonation of petroleum refinery wastewater utilizing Mn-Fe-Cu/Al_2O_3 catalyst. *Environ. Sci. Pollut. Res.* **2015**, *22*, 5552–5562. [CrossRef] [PubMed]
24. Tong, S.; Shi, R.; Zhang, H.; Ma, C. Catalytic performance of Fe_3O_4-CoO/Al_2O_3 catalyst in ozonation of 2-(2, 4-dichlorophenoxy) propionic acid, nitrobenzene and oxalic acid in water. *J. Environ. Sci.* **2010**, *22*, 1623–1628. [CrossRef]
25. Xu, B.; Qi, F.; Sun, D.; Chen, Z.; Robert, D. Cerium doped red mud catalytic ozonation for bezafibrate degradation in wastewater: Efficiency, intermediates, and toxicity. *Chemosphere* **2016**, *146*, 22–31. [CrossRef] [PubMed]
26. Chen, C.; Yu, J.; Yoza, B.A.; Li, Q.X.; Wang, G. A novel "wastes-treat-wastes" technology: role and potential of spent fluid catalytic cracking catalyst assisted ozonation of petrochemical wastewater. *J. Environ. Manage.* **2015**, *152*, 58–65. [CrossRef] [PubMed]
27. Dai, Q.; Wang, J.; Yu, J.; Chen, J.; Chen, J. Catalytic ozonation for the degradation of acetylsalicylic acid in aqueous solution by magnetic CeO_2 nanometer catalyst particles. *Appl. Catal. B* **2014**, *144*, 686–693. [CrossRef]
28. Yan, H.; Lu, P.; Pan, Z.; Wang, X.; Zhang, Q.; Li, L. Ce/SBA-15 as a heterogeneous ozonation catalyst for efficient mineralization of dimethyl phthalate. *J. Mol. Catal. A* **2013**, *377*, 57–64. [CrossRef]
29. Bing, J.; Wang, X.; Lan, B.; Liao, G.; Zhang, Q.; Li, L. Characterization and reactivity of cerium loaded MCM-41 for *p*-chlorobenzoic acid mineralization with ozone. *Sep Purif. Technol.* **2013**, *118*, 479–486. [CrossRef]
30. Moussavi, G.; Mahmoudi, M. Removal of azo and anthraquinone reactive dyes from industrial wastewaters using MgO nanoparticles. *J. Hazard. Mater.* **2009**, *168*, 806–812. [CrossRef] [PubMed]
31. Chen, C.; Yoza, B.A.; Chen, H.; Li, Q.X.; Guo, S. Manganese sand ore is an economical and effective catalyst for ozonation of organic contaminants in petrochemical wastewater. *Water Air Soil Poll.* **2015**, *226*, 182. [CrossRef]
32. Nawrocki, J.; Kasprzyk-Hordern, B. The efficiency and mechanisms of catalytic ozonation. *Appl. Catal. B* **2010**, *99*, 27–42. [CrossRef]
33. Chen, W.; Li, X.; Pan, Z.; Ma, S.; Li, L. Synthesis of MnO_x/SBA-15 for Norfloxacin degradation by catalytic ozonation. *Sep. Purif. Technol.* **2017**, *173*, 99–104. [CrossRef]
34. Pines, D.S.; Reckhow, D.A. Solid phase catalytic ozonation process for the destruction of a model pollutant. *Ozone: Sci. Eng.* **2003**, *25*, 25–39. [CrossRef]
35. Yang, L.; Hu, C.; Nie, Y.; Qu, J. Surface acidity and reactivity of β-FeOOH/Al_2O_3 for pharmaceuticals degradation with ozone: In situ ATR-FTIR studies. *Appl. Catal. B* **2010**, *97*, 340–346. [CrossRef]
36. Chen, J.; Tian, S.; Lu, J.; Xiong, Y. Catalytic performance of MgO with different exposed crystal facets towards the ozonation of 4-chlorophenol. *Appl. Catal. A* **2015**, *506*, 118–125. [CrossRef]
37. Beltrán, F.J.; Rivas, F.J.; Montero-de-Espinosa, R. A TiO_2/Al_2O_3 catalyst to improve the ozonation of oxalic acid in water. *Appl. Catal. B* **2004**, *47*, 101–109. [CrossRef]
38. Xu, R.R.; Pang, W.Q.; Yu, J.H.; Huo, Q.S.; Chen, J.S. *Chemistry Zeolites and Porous Materials*, 1st ed.; Science Press: Beijing, China, 2004; pp. 145–149. (in Chinese)
39. Rao, G.R.; Sahu, H.R. XRD and UV-Vis diffuse reflectance analysis of CeO_2-ZrO_2 solid solutions synthesized by combustion method. *J. Chem. Sci.* **2001**, *113*, 651–658.
40. Mittal, V.K.; Bera, S.; Nithya, R.; Srinivasan, M.P.; Velmurugan, S.; Narasimhan, S.V. Solid state synthesis of Mg–Ni ferrite and characterization by XRD and XPS. *J. Nucl. Mater.* **2004**, *335*, 302–310. [CrossRef]
41. Sheerin, E.; Reddy, G.K.; Smirniotis, P. Evaluation of Rh/$Ce_xTi_{1-x}O_2$ catalysts for synthesis of oxygenates from syngas using XPS and TPR techniques. *Catal. Today* **2016**, *263*, 75–83. [CrossRef]

42. Lu, X.; Huangfu, X.; Ma, J. Removal of trace mercury(II) from aqueous solution by in situ formed Mn-Fe (hydr) oxides. *J. Hazard. Mater.* **2014**, *280*, 71–78. [CrossRef] [PubMed]
43. Zhang, G.; Qu, H.; Liu, R.; Wu, R. Preparation and evaluation of a novel Fe-Mn binary oxide adsorbent for effective arsenite removal. *Water Res.* **2007**, *41*, 1921–1928. [CrossRef] [PubMed]
44. Zhang, L.; Ma, J.; Yu, M. The microtopography of manganese dioxide formed in situ and its adsorptive properties for organic micropollutants. *Solid State Sci.* **2008**, *10*, 148–153. [CrossRef]
45. Qi, F.; Xu, B.; Zhao, L.; Chen, Z.; Zhang, L.; Sun, D.; Ma, J. Comparison of the efficiency and mechanism of catalytic ozonation of 2,4,6-trichloroanisole by iron and manganese modified bauxite. *Appl. Catal. B* **2012**, *121–122*, 171–181. [CrossRef]
46. Miyakoshi, A.; Ueno, A.; Ichikawa, M. XPS and TPD characterization of manganese-substituted iron-potassium oxide catalysts which are selective for dehydrogenation of ethylbenzene into styrene. *Appl. Catal. A* **2001**, *219*, 249–258. [CrossRef]
47. Altenor, S.; Carene, B.; Emmanuel, E.; Lambert, J.; Ehrhardt, J.; Gaspard, S. Adsorption studies of methylene blue and phenol onto vetiver roots activated carbon prepared by chemical activation. *J. Hazard. Mater.* **2009**, *165*, 1029–1039. [CrossRef] [PubMed]